

OPTIMIZATION OF EARTH-MOON LOW-THRUST-ENHANCED LOW-ENERGY TRANSFER

Yuji Takubo,* Yuri Shimane,† and Koki Ho‡

This work proposes an optimization method for the novel class of lunar transfer that leverages both low-thrust acceleration and weak stability boundary effects simultaneously. Such translunar orbits are aimed at filling the gap that exists in conventional transfer options in the trade-off between the time of flight and mass ratio. We first generate the candidates for the initial guess via backward propagation from a cislunar periodic orbit. These trajectories are corrected into feasible solutions, then further optimized based on a multiple-shooting method with a Sims-Flanagan transcription. The obtained transfer time of the solutions is around 45-70 days, which is almost half of the traditional ballistic transfers (90-110 days) with a few percent increase in its propellant mass, showing a huge benefit of performing the low-thrust propulsion in the Earth-Moon low-energy transfer.

INTRODUCTION

The cislunar domain is attracting government and private interest alike as the new frontier of humanity's permanent outpost in space. As the number of activities increases, traffic to the cislunar space will become ever more frequent. Considering the complex cislunar activity as a logistics problem,¹⁻³ it is essential to have a multitude of transfer options, varying in time of flight, transfer cost, and/or realizable spacecraft (S/C) architecture. There are, up to date, two major strategies for designing impulsive transfers to the cislunar system: direct transfers and low-energy transfers (LET). Both strategies may incorporate Earth-phasing orbits and lunar flybys, allowing for a more flexible launch window and reducing the C_3 requirement on the launch vehicle.

LETs, also referred to as ballistic lunar transfers (BLT), are of particular interest due to the lower arrival specific energy with respect to the Moon compared to direct transfers.⁴⁻⁶ This results in lower lunar orbit insertion (LOI) cost at the expense of higher translunar orbit insertion (TOI) cost, which can be typically executed by the launch vehicle. The lower arrival energy is achieved by leveraging the gravitational perturbation of the Sun, as shown in Fig. 1, where the time of flight (TOF) ranges from 70 to 120 days.^{6,7} While this long TOF, combined with the high apogee, renders LETs unfavorable for crewed missions, such transfers are advantageous for robotic exploration and/or cargo delivery. In the past year alone, NASA's CAPSTONE mission, the Korea Pathfinder Lunar Orbiter (KPLO) mission, and ispace's M1 mission all utilized LETs.

In the context of low-thrust cislunar transfers, several works have leveraged invariant manifold structures of Earth-Moon L_1 libration point orbits (LPOs),⁹⁻¹¹ which results in the spiral trajectory family from the Earth. Other studies applied low-thrust propulsion systems to the lunar transfer

*Former Undergraduate Student, School of Aerospace Engineering, Georgia Institute of Technology, Atlanta, GA 30332.

†Ph.D. Candidate, School of Aerospace Engineering, Georgia Institute of Technology, Atlanta, GA 30332.

‡Assistant Professor, School of Aerospace Engineering, Georgia Institute of Technology, Atlanta, GA 30332.

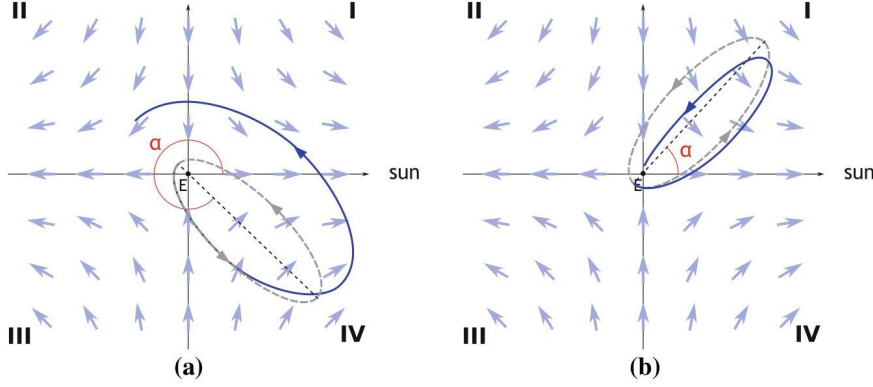


Figure 1: Influence of tidal forces over the S/C trajectory in Sun-Earth rotating frame.⁸

with indirect method¹² or reinforcement learning-based approach.¹³ Multiple papers studied Earth-Moon low-energy low-thrust transfers, however the primary usage of the low-thrust propulsion has been limited to the lunar capture phase of the transfer.^{14,15} Parrish considered the addition of ΔV to the LET to the Earth-Moon L_2 rectilinear Halo orbit (NRHO), while the application is limited to the correction maneuver but not the overall optimal transfer with the propulsion system.¹⁶ To support prosperous human activities in the cislunar region, it is preferable to have a wide range of transfer options, trading off the transfer cost and TOF.⁸ It is evident that there is a gap in transfer options between direct transfers and LETs.

The proposed work aims to uncover transfers of this “intermediate” range by introducing low-thrust acceleration. This strategy essentially enhances the effect of the Sun-perturbation,^{17,18} as though the Sun had a greater gravitational acceleration; hence, this class of transfers is named “enhanced low-energy transfers (ELET)”. The idea of integrating LET and low-thrust propulsion to reach Earth-Moon L_2 periodic orbits is examined by Scheuerle et al.,¹⁹ while the search of the trajectory families is based on the correction scheme (i.e., natural parameter continuation).

The primary contribution of this paper is in the optimization method for this new type of transfer. First, initial guess candidates are generated based on the grid search with the pre-determined policy of the thrusting directions. Next, the collected initial guess candidates are corrected into feasible trajectories that satisfy terminal conditions at the LPO and LEO. Finally, the corrected initial guesses are used as initial guesses of the optimization that locally minimizes the TOF, providing the trade-off of the added system mass and the reduced TOF. In order to perform the correction and optimization, a multiple-shooting scheme based on Sims-Flanagan transcription (SFT)²⁰ is developed.

PROBLEM DESCRIPTION AND OVERALL APPROACH

In this paper, the optimal control from the Earth’s parking orbit to the lunar periodic orbit is considered. The trajectory optimization problem for ELETs entails two important characteristics. First, the trajectory is generated in the four-body system comprised of the Sun, Earth, Moon, and S/C. The dynamics in this system are extremely sensitive, so the forward propagation and backpropagation of the dynamics, especially around the celestial bodies, would create a nonnegligible numerical inconsistency. This motivates the tailored numerical method for efficient convergence of the correction and optimization. The second characteristic is that the S/C may exert low-thrust propulsion in the dynamical system. Due to the continuous thrust policy, the optimal control problem with

time-variant thrust is underlined in the problem. Moreover, such an optimization problem is highly nonlinear and multi-modal, which raises another question about the search for a good initial guess in order to reach the local optimum quickly.

The summary of the method that is developed in this paper is as follows:

- Dynamics and coordinate frame: bi-circular restricted four-body problem (BCR4BP) in the Sun- B_1 rotating frame.
- Initial guess candidate search: grid-search with backward propagation from the LPO.
- Correction from the initial guess candidate to a feasible initial guess: multiple-shooting based on SFT, solved by a nonlinear optimizer (SNOPT²¹).
- Optimization: minimizing TOF, multiple-shooting based on SFT, solved by a nonlinear optimizer (SNOPT).

In the following sections, each component that comprises the proposed method is elaborated.

DYNAMICAL SYSTEMS MODELING

When designing low-energy transfers in cislunar space, the effect of the Earth, Moon, and Sun must all be taken into account. At the preliminary design stage, this is commonly done by either patching the Sun-Earth circular restricted three-body problem (CR3BP) and Earth-Moon CR3BP in a fashion similar to patched-conics design^{4,22–24} or by considering the bi-circular restricted four-body problem (BCR4BP).^{7,25–31} In this paper, the BCR4BP is adopted to describe the S/C dynamics in the Earth-Moon system, as it provides a more intuitive frame in which the trajectory of a LET can be studied compared to the Earth-Moon rotating frame-based dynamics. This will be particularly critical when defining heuristic thrust policies for generating initial guess candidates, which will be discussed further in the subsequent section.

Normalization

The normalization (non-dimensionalization) of the length, mass, and time is performed to ensure favorable numerical behavior. Let m_E , m_L , and m_s be the dimensional masses of the Earth, Moon, and Sun. The nondimensional parameters are summarized in Table. 1.

Table 1: Nondimensional parameters in the Sun-Earth-Moon system

Notation	Definition	Value
m^*	$m_E + m_L$	6.046×10^6 kg
l^*	Earth-Moon distance	3.8475×10^5 km
t^*	(one sidereal day) / 2π	4.06075×10^4 s

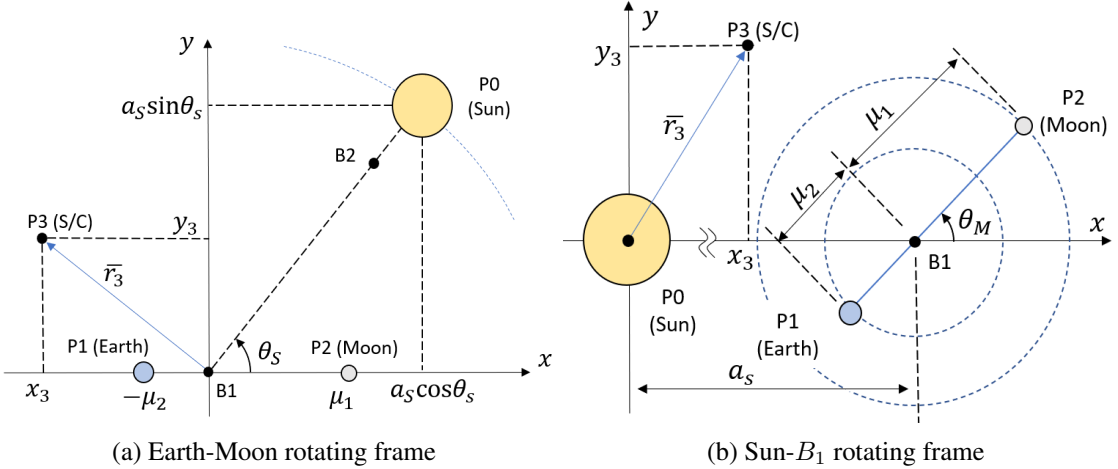


Figure 2: Coordinate frames for BCR4BP

With the nondimensional parameters, the mass of the Earth, Moon, and Sun are scaled as follows:

$$\begin{aligned}\mu_1 &= \frac{m_E}{m^*} \\ \mu_2 &= \frac{m_L}{m^*} = 1 - \mu_1 \\ \mu_S &= \frac{m_s}{m^*}.\end{aligned}\tag{1}$$

Note that due to the normalization, the Earth- B_1 distance and Moon- B_1 distance, where B_1 is the Earth-Moon barycenter, are equivalent to μ_2 and $1 - \mu_2$, respectively. Additionally, we introduce a parameter to express the distance between the Sun and Earth-Moon system as follows:

$$a_s = \frac{(\text{Sun-}B_1 \text{ distance})}{l^*}\tag{2}$$

Equations of Motion

There exist two prominent coordinate frames for the BCR4BP. One is based on the Earth-Moon rotating frame that adds gravitational perturbation from the Sun, which is assumed to be rotating around the Earth-Moon barycenter B_1 in a circular manner. Assuming that the Sun- B_1 rotation and the Earth-Moon rotation are co-planar, the BCR4BP in the Earth-Moon rotating frame is presented in Fig. 2a. The other approach is to consider the dynamics in the Sun- B_1 rotating frame. Under the coplanar assumption, the coordinate frame is shown in Fig. 2b. This coordinate frame further assumes that the origin of the rotation is at the Sun but not at B_1 ; this assumption enables these two coordinate frames to be completely equivalent through an adequate rotation.

Using the coordinate system of the rotating frame, the relationship between the second-order derivative in the inertial frame and the synodic frame is written as

$${}^I \left(\frac{d^2}{dt^2} \vec{r} \right) = {}^b \left(\frac{d^2}{dt^2} \vec{r} \right) + 2\vec{\omega} \times {}^b \left(\frac{d}{dt} \vec{r} \right) + \vec{\omega} \times (\vec{\omega} \times {}^b \vec{r}) = \frac{\vec{F}}{m},\tag{3}$$

where ${}^I(\cdot)$ is the state representation in the inertial frame, and ${}^b(\cdot)$ is that in the rotating frame that shares the same origin with the inertial frame. Resolving this in the Sun- B_1 rotating frame, the coordinates of the S/C $[x_3, y_3, z_3]$ and their derivatives, the equations of motion become as follows:

$$\begin{aligned}\ddot{x}_3 &= x_3 + 2\dot{y}_3 + \frac{F_x}{m} \\ \ddot{y}_3 &= y_3 - 2\dot{x}_3 + \frac{F_y}{m} \\ \ddot{z}_3 &= \frac{F_z}{m}.\end{aligned}\tag{4}$$

The vector components of the external force \vec{F} resolved in the Sun- B_1 frame are given by

$$\begin{aligned}\frac{F_x}{m} &= -\frac{\mu_S}{r_{30}^3}x_3 + \frac{\mu_1}{r_{31}^3}[a_s + x_E - x_3] + \frac{\mu_2}{r_{32}^3}[a_s + x_L - x_3] + \frac{T_x}{m} \\ \frac{F_y}{m} &= -\frac{\mu_S}{r_{30}^3}y_3 + \frac{\mu_1}{r_{31}^3}(y_E - y_3) + \frac{\mu_2}{r_{32}^3}(y_L - y_3) + \frac{T_y}{m} \\ \frac{F_z}{m} &= -\frac{\mu_S}{r_{30}^3}z_3 + \frac{\mu_1}{r_{31}^3}(z_E - z_3) + \frac{\mu_2}{r_{32}^3}(z_L - z_3) + \frac{T_z}{m} \\ r_{30} &= \sqrt{x_3^2 + y_3^2 + z_3^2} \\ r_{31} &= \sqrt{(x_3 - x_E)^2 + (y_3 - y_E)^2 + (z_3 - z_E)^2} \\ r_{32} &= \sqrt{(x_3 - x_L)^2 + (y_3 - y_L)^2 + (z_3 - z_L)^2}\end{aligned}\tag{5}$$

where the terms are ordered as Sun-gravity, Earth-gravity, Moon-gravity, and the acceleration by the thrust in the Sun- B_1 rotating frame $[T_x, T_y, T_z]$; r_{ij} is the scalar distance from point i to j , where $i, j = 0, 1, 2, 3$ represents the Sun, Earth, Moon, and S/C, respectively; finally, m is the spacecraft mass. The position of the Earth and Moon with respect to B_1 is given by $[x_E, y_E, z_E]$ and $[x_L, y_L, z_L]$. Under the assumption of coplanar BCR4BP, these coordinates are expressed as follows:

$$\begin{bmatrix} x_E \\ y_E \\ z_E \end{bmatrix} = \begin{bmatrix} -\mu_2 \cos \theta_M \\ -\mu_2 \sin \theta_M \\ 0 \end{bmatrix}, \quad \begin{bmatrix} x_L \\ y_L \\ z_L \end{bmatrix} = \begin{bmatrix} (1 - \mu_2) \cos \theta_M \\ (1 - \mu_2) \sin \theta_M \\ 0 \end{bmatrix},\tag{6}$$

where θ_M is the Moon's phase in the Sun- B_1 frame, which is the Moon- B_1 line with respect to the x -axis in the Sun- B_1 rotating frame, as shown in Fig. 2b. This is derived from the angular velocity of the Moon around B_1 , ω_M , as

$$\theta_M = \theta_{M,0} + \omega_M t,\tag{7}$$

where $\theta_{M,0}$ is the Moon's phase at the initial epoch. Note that the dependence of θ_M on time makes the four-body dynamics a non-autonomous system. A comprehensive discussion of the dynamical systems in the BCR4BP is summarized in.³¹

In addition to position and velocity, the evolution of mass is expressed in the following differential equation:

$$\dot{m} = -\frac{T_{\max}}{I_{sp}g}\tau,\tag{8}$$

where T_{\max} is a thrust magnitude, I_{sp} is a specific impulse, g is the standard gravity, and $\tau \in [0, 1]$ is the control throttle.

In the remainder of this paper, all trajectories are plotted in the Sun- B_1 rotating frame with the origin shifted to B_1 . Furthermore, the term *quadrant* refers to the one defined in this coordinate frame, as shown in Fig. 3b.

INITIAL GUESS CANDIDATES GENERATION

The database of initial guess candidates is generated using heuristic thrust policies that are hypothesized to “enhance” the LETs by reducing the TOF at the cost of some propellant expenditure. Grid search is performed through the terminal state at the LPO, where the trajectories are propagated in $-t$ direction and filtered based on criteria that keep potentially-feasible Earth-Moon transfers.

Given the geometry of the LPO, the terminal position in the orbit \mathbf{r}_{LPO} can be defined by two parameters: $\theta_{M,LPO}$ and ϕ_{LPO} . $\theta_{M,LPO}$ is the Moon’s phase at the arrival epoch. ϕ_{LPO} parameterizes the phase in the LPO, defined as $\phi_{LPO} = t_{LPO}/P \in [0, 1]$, where P is the period of the LPO, and t_{LPO} is the propagation time from a reference point. In this work, the orbit state in CR3BP that is closer to the Earth among two intersections of the orbit and the $x - z$ plane in the Earth-Moon rotating frame serves as the reference point.

The terminal velocity \mathbf{v}_{LPO} is automatically defined based on the eigenvector direction of the state transition matrix at \mathbf{r}_{LPO} that generated in CR3BP.⁹ Additional parameters ϵ_r, ϵ_v are defined, which are the coefficients applied to the direction of the eigenvalues of the state transition matrix at the given departure position in the orbit to generate the terminal states. Note that all trajectories are propagated with the BCR4BP, so the given direction will not be on the surface of the exact invariant manifold. However, the energetically-free insertion into the LPO due to the weak stability boundary effect is reasonably expected by defining the \mathbf{v}_{LPO} in this fashion.

When generating the initial guesses, the maximum thrust is always applied to the S/C by default. Assuming the existence of a thrust direction that reduces the TOF at any state, the thrust history of the minimum TOF trajectory would also be close to full-throttle for the entire transfer. Therefore, a well-informed initial guess of the thrust direction is available, maintaining full-throttle on the low-thrust propulsion constitutes a rational conjecture.

Nevertheless, we pose two phases that the S/C coasts ballistically. First, the thrust is turned off for a certain period before the arrival at the LPO. This way, the S/C can successfully leverage the weak stability boundary effect and perform the energetically-free orbit insertion to the LPO. Additionally, thrusting is not allowed during the Launch and Early Orbit Phase (LEOP). Thrusting in this period is likely to be undesirable as the S/C performs the mission necessitate system checks. This constraint is realized by turning off the thrust when the range of the S/C from B_1 in the backpropagated trajectory is shorter than the Moon- B_1 distance; this phase corresponds to the launch from the Earth’s parking orbit when propagating the dynamics in the forward direction. It is also worth noting that thrusting in the LEOP is ineffective (except for a targeting maneuver) because the launch velocity is relatively high and the S/C reaches the Moon’s semi-major axis in about 3 days; low-thrust propulsion would not be able to apply enough ΔV in this short period of time.

Note that there are other methods to explore the solution space, such as natural parameter continuation.¹⁹ While it can present the evolution of the trajectory family from a chosen one, it is also a non-trivial task to find such an initial trajectory to start with. Additionally, it is difficult to discuss the optimality of the obtained trajectory family, which is the primary reason this method is not

adopted in this work.

Heuristic Thrust Directions

We develop four heuristics of the thrust direction policy to generate the initial guess candidates, which effectiveness is compared in this work. In this subsection, the derivation of each thrust direction and the rationale behind the selection of it is discussed.

Tangent to B_1 The first policy considered is to apply the force in a tangential direction to B_1 . In the Sun- B_1 rotating frame, the S/C velocity is almost radial to B_1 after the launch, and gradually increases the tangential component as it approaches the LPO, which is represented as a circular motion around B_1 . Additionally, the tidal force exerted on the S/C at apoapsis is nearly tangential to B_1 . Based on this observation, the proposed policy was considered to be effective as this thrust direction is augmenting the tidal force at the apoapsis in the second and fourth quadrants and supports the overall rotating motion of the S/C around B_1 . Therefore, the thrust direction is expressed as

$$\hat{\mathbf{i}}^* = {}_{\text{Sun-}B_1 \text{ rot.}} \left(\frac{\hat{\mathbf{z}} \times (\mathbf{r}_{\text{S/C}} - \mathbf{r}_E)}{|\hat{\mathbf{z}} \times (\mathbf{r}_{\text{S/C}} - \mathbf{r}_E)|} \right), \quad (9)$$

where $\hat{\mathbf{z}} = [0, 0, 1]^T$, and ${}^{\text{Sun-}B_1 \text{ rot.}}(\cdot)$ represents the state resolved in the Sun- B_1 rotating frame.

Velocity direction in the Sun- B_1 frame Another simple heuristic that can be considered is to thrust in the direction that accelerates the S/C velocity at each moment. In spite of its simplicity, the thrust direction aligns with that of the tidal force at apoapsis, which reduction of TOF can be expected.

$$\hat{\mathbf{i}}^* = {}_{\text{Sun-}B_1 \text{ rot.}} \left(\frac{\mathbf{v}_{\text{S/C}}}{|\mathbf{v}_{\text{S/C}}|} \right) \quad (10)$$

Maximization of Jacobi Constant Scheuerle et al. discussed the thrust direction from the perspective of energy.¹⁹ The increase in the instantaneous Jacobi constant in the Earth-Moon rotation frame, which represents the energy in the Earth-Moon-S/C three-body system, is observed throughout the transfer and the proposed thrust direction policy was to apply the thrust direction that maximizes it.

$$JC = 2U - (\dot{x}^2 + \dot{y}^2 + \dot{z}^2) \quad (11)$$

$$\text{where } U = \frac{1}{2}(x^2 + y^2) + \frac{1 - \mu_2}{r_{13}} + \frac{\mu_2}{r_{23}} \quad (12)$$

It is derived that the maximizing direction of the instantaneous Jacobi constant is the anti-velocity direction of the S/C in the Earth-Moon rotating frame. Therefore, the thrust direction is expressed as

$$\hat{\mathbf{i}}^* = \underset{\gamma, \beta}{\operatorname{argmax}} {}^{\text{E-M rot.}} \left(\frac{dJC_{\text{inst}}}{dt} \right) = - {}^{\text{E-M rot.}} \left(\frac{\mathbf{v}_{\text{S/C}}}{|\mathbf{v}_{\text{S/C}}|} \right), \quad (13)$$

where ${}^{\text{E-M rot.}}(\cdot)$ represents the state representation in the Earth-Moon rotating frame.

Tidal force Direction The final thrust policy is to apply the thrust along the Sun-perturbation i.e., tidal force. The fundamental factor that realizes the Earth-Moon LET in the four-body problem is due to this acceleration at the second and fourth quadrant in the Sun- B_1 frame, as shown in Fig. 1. Hence, this thrust policy enhances the magnitude of the Sun-perturbation that is exerted on the S/C. The tidal force applied to the S/C is expressed as follows:⁸

$$\mathbf{F}_{\text{tidal}} = \frac{\mu_S}{R^3} \left[\hat{\mathbf{R}} \hat{\mathbf{R}}^T - \mathbf{I}_{3 \times 3} \right] (\mathbf{r}_{S/C} - \mathbf{r}_E) \quad (14)$$

where \mathbf{R} is the Sun-Earth distance vector, R is its norm, and $\hat{\mathbf{R}} := \mathbf{R}/R$. Furthermore, $\mathbf{r}_{S/C}$ and \mathbf{r}_E are the S/C and Earth position vector, respectively. Therefore, the thrust direction is defined as follows:

$$\hat{\mathbf{i}}^* = \text{Sun-}B_1\text{rot.} \left(\frac{\mathbf{F}_{\text{tidal}}}{|\mathbf{F}_{\text{tidal}}|} \right). \quad (15)$$

OPTIMIZATION METHOD

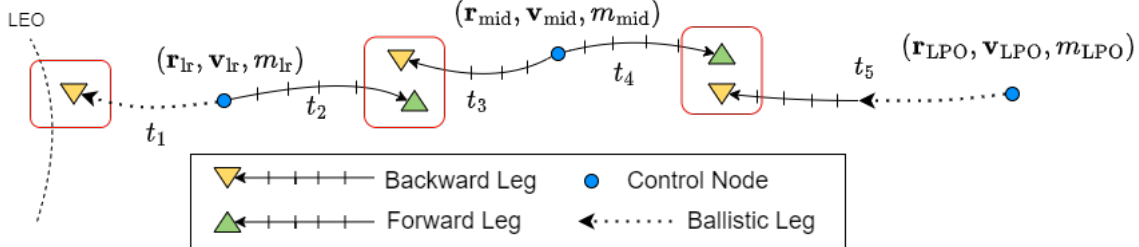
Providing a feasible solution to an optimizer contributes to its convergence, especially for problems with sensitive nonlinear constraints. However, the initial guess candidates discussed in the previous section have a wide range of periapsis altitudes, which are not strictly feasible. Therefore, we first generate a batch of feasible trajectories via a correction process, followed by an optimization step. Although the first correction process could be skipped if a good initial guess was obtained, having this step not only provides a more efficient convergence of the optimization but also accommodates a broader exploration of the initial guess candidates. The following subsections elaborate on the multiple-shooting scheme with SFT, and discuss the constraints and objectives of the optimization problem.

Multiple-Shooting Method

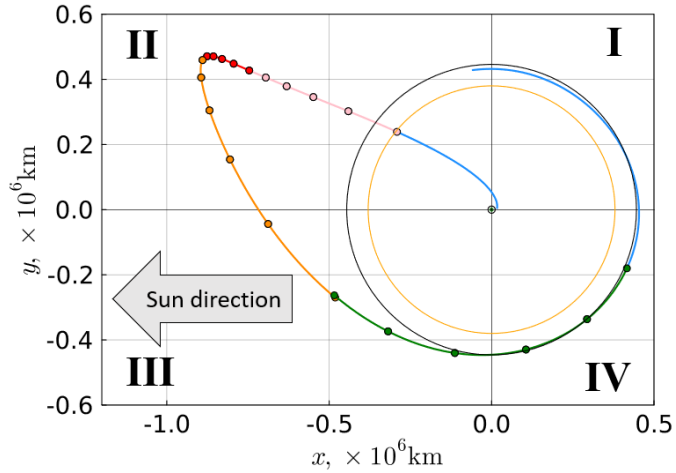
The correction of the initial guess candidates and the optimization are done via a direct method; trajectories are discretized into a finite number of arcs and converted to the parameter optimization problem. In this work, a multiple-shooting scheme based on SFT is developed as shown in Fig. 3. The design variable vector \mathbf{x} comprises the following elements:

$$\begin{aligned} \mathbf{x} &= [\mathbf{x}_{lr}, \mathbf{x}_{mid}, \mathbf{x}_{LPO}] \\ \mathbf{x}_{lr} &= [\mathbf{r}_{lr}, \mathbf{v}_{lr}, m_{lr}, t_1, t_2, \boldsymbol{\tau}_2] \\ \mathbf{x}_{mid} &= [\mathbf{r}_{mid}, \mathbf{v}_{mid}, m_{mid}, t_3, t_4, \boldsymbol{\tau}_3, \boldsymbol{\tau}_4] \\ \mathbf{x}_{LPO} &= [\theta_{M,LPO}, \phi_{LPO}, t_5, \boldsymbol{\tau}_5] \\ \boldsymbol{\tau}_j &= [\tau_1^j, \gamma_1^j, \beta_1^j, \dots, \tau_k^j, \gamma_k^j, \beta_k^j, \dots, \tau_n^j, \gamma_n^j, \beta_n^j], k \in [1, n]. \end{aligned} \quad (16)$$

First, \mathbf{r}_{lr} , \mathbf{v}_{lr} , and m_{lr} describes the control node placed around the lunar radius. The forward propagation from the LEO state could be extremely sensitive as the initial state is very close to the Earth. This is alleviated by placing a control node relatively far from the Earth and then backpropagating to the LEO state from it, which provides numerical stability and faster convergence of optimization. Another control node is placed around the apoapsis with respect to the Earth to improve the convergence, which states are described in \mathbf{r}_{mid} , \mathbf{v}_{mid} , and m_{mid} . Finally, $\theta_{M,LPO}$ and ϕ_{LPO} define the LPO



(a) Propagation directions, control nodes, and match points



(b) A sample initial guess candidate transcribed into the multiple-shooting scheme. The yellow circle is the Moon orbit, the black dot at the center is B_1 , and the exterior black circle is the Earth-Moon L_2 . The center of x -coordinates is shifted to B_1 . The quadrants are shown in Roman numerals.

Figure 3: Multiple-shooting method

state, as discussed in the previous section. In this formulation, the terminal mass of the S/C at the LPO is set to be constant, therefore excluded from the design variables.

The throttle of the engine is parameterized by $\tau_k^j \in [0, 1]$, $j = 2, 3, 4, 5$ (i.e., $T = \tau_k^j T_{\max}$), and γ_k^j and β_k^j represent the angles that determine the direction of the thrust, where n is the number of segments allocated for each leg. Note that there is no τ_1 because the leg corresponding to t_1 is ballistic due to the LEOP, and for planar problems, $\beta_k^j = 0$ holds. Finally, $t_j, j = 1, 2, \dots, 5$ are the norms of the propagation time assigned for each leg, as shown in Fig. 3a. Note that the final leg with the transfer time t_5 is divided into two different legs; the final arrival leg is ballistic, and the remaining arc is a trusted arc. The predefined coasting duration is the same as the value used for the initial guess candidate generation.

A sample trajectory transcribed from the initial guess candidate into the multiple-shooting scheme is shown in Fig. 3b. The trajectory is reconstructed from the continuous

trajectory, the positional error in the yellow and green leg is confirmed. This exemplifies the numerical inconsistency of forward propagation and backward propagation.

Optimization Problem

The trajectory optimization problem is written as follows, using the aforementioned multiple-shooting method:

$$\min_{\mathbf{x}} \quad \mathcal{J}(\mathbf{x}) \quad (17)$$

$$\text{such that } \|\mathbf{r}_{lr}(-t_1)\|_2 = r_{LEO} \quad (18)$$

$$(\mathbf{r}_{lr}(-t_1) - \mathbf{r}_E) \cdot \mathbf{v}_{lr}(-t_1) = 0 \quad (19)$$

$$[\mathbf{r}_{lr}(t_2), \mathbf{v}_{lr}(t_2), m_{lr}(t_2)] = [\mathbf{r}_{mid}(-t_3), \mathbf{v}_{mid}(-t_3), m_{mid}(-t_3)] \quad (20)$$

$$[\mathbf{r}_{mid}(t_4), \mathbf{v}_{mid}(t_4), m_{mid}(t_4)] = [\mathbf{r}_{LPO}(-t_5), \mathbf{v}_{LPO}(-t_5), m_{LPO}(-t_5)]. \quad (21)$$

First, Eq. 18 constrains the departure state at the Earth's parking orbit to be at a certain altitude. Additionally, Eq. 19 requires the departure state to be tangent to the Earth (and the parking orbit). Eq. 20 and 21 enforce the continuation of the states at each break point, as shown in Fig. 3a.

Due to the pronounced nonlinearity of the dynamics, finding a feasible solution space for this problem itself is already non-trivial. Hence, a generalized nonlinear optimizer SNOPT²¹ is adopted for the correction process. A constant objective, low feasibility tolerance, and high optimality tolerance lead SNOPT to modify the design variables, which are originally infeasible, into the feasible domain. Only constraints Eqs. 18 - 21 are considered in the correction process as the primary purpose of this process is to generate a batch of feasible solutions that can serve as an initial guess for further optimization.

It is of particular interest in this work to search for the minimum TOF transfer. Therefore the objective for the optimization is set to $\mathcal{J}(\mathbf{x}) = \text{TOF} = \sum_{i=1}^5 t_i$. Note that the scaling of the variables and constraints is critical for robust convergence in a sensitive solution space. For this problem, we normalize the S/C mass based on the arrival mass to avoid the numerical instability if it is normalized by m^* . As shown in the following section, even after this treatment, the normalized S/C mass \tilde{m} consumes its propellant in the order of 10^{-2} , while the remaining states vary in the order of 10^0 . The variables are further scaled properly so that all variables and constraints fed to the optimization solver have a similar order of magnitude.

RESULTS AND ANALYSIS

The collected batches of trajectories and optimized representative solutions are presented in this section. As a case study, the transfer from LEO ($r_{LEO} = 6,875$ km) to an Earth-Moon L_2 Lyapunov orbit with a period of 14.82956 days is considered; the properties of the orbit are summarized in Table 2. Note that this leads to the entire problem being two-dimensional, and therefore $\beta_j^k = 0 \forall k, j$ holds for the following discussion. Furthermore, the low-thrust propulsion system is assumed to have $T_{\max} = 0.4$ N and $I_{sp} = 2,500$ s. Finally, the arrival mass at the LPO is set to $m_{LPO} = 2,500$ kg.

To make a bundle of initial guess candidates, the two-dimensional grid space of $\theta_{M,LPO}$ and ϕ_{LPO} are generated, where $\theta_{M,LPO}$ is discretized by 60, and ϕ_{LPO} is discretized by 300; this leads to the generation of 18,000 trajectories for each thrust policy. Additionally, the coefficients for the arrival

x_0	y_0	z_0	v_{x0}	v_{y0}	v_{z0}	period	stability index
1.122687986019680	0.0	0.0	0.0	0.1650993133797783	0.0	3.41036	618.761847

Table 2: Earth-Moon Lyapunov orbit parameter (normalized, coordinates are in Earth-Moon rotating frame (Fig.2a)).

velocity at LPO are set to $\epsilon_r = \epsilon_v = 1e-5$. The terminal coasting duration towards the arrival state at the LPO is set to 10 days.

Among the generated trajectories, ones with the first periapsis radius to the Earth in $3,000 \leq r_p \leq 30,000$ km are kept as good initial guess candidates. Additionally, considering the realistic launch direction, only trajectories with positive z -component of the angular momentum at their periapsis states are preserved. This filters out the trajectories that are launched in the opposite direction to the Earth’s rotation. Moreover, we allow the lunar flybys up to once right after the launch and do not consider the trajectories that have flybys around at the arrival phase. Compared to the lunar flyby a few days after the launch, ones that happen in the final few weeks of the transfer have a much smaller relative velocity to the Moon, requiring the consideration of flyby in a multi-body regime. The proposed transcription cannot handle this, and trajectory optimization with such “slow” flybys is left to future research. Finally, the trajectories that have multiple apoapsides are eliminated from the initial guess candidates because not only such a geometry is also not compatible with this transcription scheme but the TOFs of the transfers are usually much longer.

Corrected Trajectory families

The trajectory families generated by the grid search and the following correction are shown in Fig. 4. The color of the trajectories represents the TOF of the transfers. Note that these trajectories no longer follow the exact thrust policies after the correction, while they retain the overall structure of the families generated via the grid search. Various geometries of trajectories can be found in each thrust policy.

First, trajectories that are corrected from the no-thrust policy (i.e., BLT) have TOFs in the range of 90 to 110 days (Fig.4a), which agree with the values from past literature. On the contrary, all feasible trajectories that use the low-thrust propulsion enjoyed a significant reduction in the TOF, including the 45-day transfer for the shortest with the thrust in the max. JC_{inst} direction (Fig. 4d). Among the four thrust heuristics that we hypothesized, thrusting in max. JC_{inst} direction clearly outperforms the other options in terms of TOF. Trajectories that have less than 50 days of TOF are only found in the max. JC_{inst} direction and the tangential direction with respect to B_1 .

Another important observation is the emergence of the transfers which apoapsides lay on the first and third quadrants in the Sun- B_1 frame, which has not been observed to the best of our knowledge. While these transfers do not leverage the natural dynamical system, the low-thrust propulsion is resisting the disadvantageous tidal force direction in the first and third quadrants, which still leads to shorter TOFs.

The launch and arrival properties of the obtained trajectories are presented in Fig. 5. First, a widely distributed launch window is observed from Fig. 5a, being available at almost any time. On the contrary, Fig. 5b shows that the distribution of the arrival geometry of the Sun, Earth, and Moon is not uniform, where the transfers are almost prohibitive in $90 \leq \theta_{M,LPO} \leq 135^\circ$ and $270 \leq \theta_{M,LPO} \leq 325^\circ$. Fig. 5c combines the previous two plots and correlates the departure

Moon angle $\theta_{M,\text{LPO}}$ and the arrival Moon angle $\theta_{M,\text{LPO}}$. It is confirmed that the thrust policies are insensitive to $\theta_{M,\text{LEO}}$ to reach a certain reachable $\theta_{M,\text{LPO}}$.

The arrival state at the LPO is also an important metric from the mission design perspective because diversity in the arrival state will expand the choices in its mission operation. Fig. 5d represents the distribution of the solutions corresponding to ϕ_{arr} , the indicator of the phase in the LPO when the S/C is inserted into it. We can observe that each thrust policy has a distinct range of arrival points, where the ballistic transfers, transfers with max. JC_{inst} direction and those with tidal force direction prefer the first half of the LPO from the intersection of the orbit and $x - z$ plane that is closer to the Earth (i.e., $y \geq 0$ in the Earth-Moon rotating frame), while the trajectories with the tangential thrust to B_1 and those with the thrust in velocity direction choose the second half of the LPO as their arrival states.

Optimized trajectories from the representative solution points

The solutions with the minimum TOF from each thrust policy are chosen as representative trajectories to validate the performance of the proposed optimization scheme. Fig. 6 presents the distribution of the TOF and the departure mass normalized by the arrival mass (2,500 kg), \tilde{m}_{LEO} , which are the key objectives for the preliminary mission design; the minimum TOF solutions are presented in white marks. A linear relationship between the TOF and m_{LEO} is generally observed because we enforced the S/C to full-throttle its thrust when generating the initial guess candidates. Note that there are some exceptions for a number of trajectories with the thrust along the velocity direction in the Sun- B_1 frame and one trajectory corrected from the BLT. This is because the scattered trajectories are corrected from the initial guess candidates with free TOF and \tilde{m}_{LEO} , where some of them converged to a trajectory that has drastically different geometry or thrust profile to the corresponding initial guess candidate.

Fig. 7, 8, 9, and 10 illustrate the optimized representative trajectories with a thrust quiver and the initial guess. The thick parts in the optimized trajectories represent the arcs where the thrust is performed (i.e., $\tau_k^j > 0$). Furthermore, the history of the in-plane thrust angle measured from the x -axis of the Sun- B_1 rotating frame is represented as $\bar{\gamma}$. The in-plane thrust angle obtained from the optimized trajectory is shown in the blue solid line, and the thrust angle corresponding to the heuristic policy along the optimized trajectory is shown in the pink dotted line. Comparing the two thrust angle histories, it is possible to study how much the optimized thrust policy is shifted from the hypothesized heuristic trust direction. Finally, the in-plane thrust angle of the initial guess trajectory is shown as the green solid line.

The values of TOF and departure mass of the corrected initial guess and the optimized trajectory are shown in Table 3. First, all trajectories successfully converged with a lower TOF than that of the corresponding initial guess, except for the one with the thrust along with tangential direction to B_1 . This can be attributed to the multi-modal solution space, where the solution shifted to the other local optima. As the optimization solver still exited with optimality while the shift in the TOF is only less than 0.3 days, the entire solution space is considered to be highly multi-modal. Moreover, since \tilde{m}_{LEO} decreased after the optimization, the optimized solution is most likely shifted from a local optimum that is on the Pareto front of TOF and \tilde{m}_{LEO} , which has a slightly larger TOF than the initial guess. Interestingly, the departure mass of all optimized solutions is decreased via optimization. Since the original initial guess candidates are generated with the full-throttle low-thrust propulsion, the decrease in TOF is considered to reduce the time of burn, resulting in a smaller departure mass.

Table 3: Optimizatoin results of the representative trajectories (min TOF solutions from each thrust policy)

Thrust policy		TOF, days	\tilde{m}_{LEO}
Tangent to B_1	initial guess	49.691	1.0209
	optimal	49.953	1.0184
S/C Velocity (Sun- B_1 rot.)	initial guess	51.578	1.0217
	optimal	50.125	1.0178
max. JC_{inst}	initial	46.725	1.0193
	optimal	45.746	1.0166
Tidal force	initial	52.105	1.0223
	optimal	50.412	1.0184

Even though each trajectory falls into a different local optimum, several similarities in the (locally) optimal thrust policy can be discussed. First, all optimized trajectories decided to turn off the thrust for the first few days even after the S/C passes the Moon’s semi-major axis. It is considered that the thrust in the arc before the apoapsis does not contribute to the reduction of TOF. On the contrary, the thrusts are added around and after the apoapsis, where the velocity of the S/C is much smaller than right after the launch, for all optimized trajectories in the direction that enhances the tidal force (Fig. 1). However, as illustrated in Fig. 10b, the optimal thrust direction completely differs from the tidal force direction when the S/C enters the first and third quadrants. This is the primary reason that the trajectories along with the tidal force are not necessarily the best heuristic thrust policy with respect to the minimization of TOF compared to the thrust of max. JC_{inst} direction or that in the tangential direction to B_1 .

CONCLUSION

The trajectory optimization scheme for the low-thrust-enhanced low-energy transfer, ELET, in the Sun-Earth-Moon system is presented in this paper. The three-staged process of initial guess candidate search via grid search, correction process, and the final optimization successfully unveils the new Earth-Moon transfer type whose TOF ranges from 45 to 70 days in compensation of a few percent of the increase in mass. These transfers are locally optimal in the sense of minimum TOF and disclose the potential for low-thrust propulsion-enhanced transfers to fill the gap in existing translunar trajectory options in terms of TOF.

Augmentation of the low-energy transfer with the low-thrust propulsion will certainly contribute to future activities in the cislunar domain, and further investigation for fast and efficient trajectory design in such a complex dynamical system is expected. Also, fast approximation of such transfers is critical for the integration of various transfer options into future space logistics problems. The exploration of the various heuristic thrust policy in this work can enable their use for further trade study and optimization of such transfers.

REFERENCES

- [1] H. Chen and K. Ho, “Integrated space logistics mission planning and spacecraft design with mixed-integer nonlinear programming,” *Journal of Spacecraft and Rockets*, Vol. 55, No. 2, 2018, pp. 365–381.

- [2] B. B. Jagannatha and K. Ho, “Optimization of in-space supply chain design using high-thrust and low-thrust propulsion technologies,” *Journal of Spacecraft and Rockets*, Vol. 55, No. 3, 2018, pp. 648–659, 10.2514/1.A34042.
- [3] Y. Takubo, H. Chen, and K. Ho, “Hierarchical reinforcement learning framework for stochastic space-flight campaign design,” *Journal of Spacecraft and Rockets*, Vol. 59, No. 2, 2022, pp. 421–433.
- [4] W. S. Koon, M. W. Lo, J. E. Marsden, and S. D. Ross, “Low energy transfer to the Moon,” *Celestial Mechanics and Dynamical Astronomy*, Vol. 81, No. 1-2, 2001, pp. 63–73, 10.1023/A:1013359120468.
- [5] E. Belbruno, “Analytic estimation of weak stability boundaries and low energy transfers,” *Celestial Mechanics, Dedicated to Donald Saari for his 60th Birthday*, Vol. 292, 2002, p. 17.
- [6] J. S. Parker and R. L. Anderson, *Low-Energy Lunar Trajectory Design*. Hoboken, New Jersey: Wiley, 2014.
- [7] F. Topputo, “On optimal two-impulse Earth–Moon transfers in a four-body model,” *Celestial Mechanics and Dynamical Astronomy*, Vol. 117, No. 3, 2013, pp. 279–313.
- [8] R. Capuzzo-Dolcetta and M. Giacconi, “A study of low-energy transfer orbits to the Moon: towards an operational optimization technique,” *Celestial Mechanics and Dynamical Astronomy*, Vol. 115, No. 3, 2013, pp. 215–232.
- [9] C. Martin and B. A. Conway, “Optimal low-thrust trajectories using stable manifolds,” *Spacecraft Trajectory Optimization*, 2010, pp. 238–262.
- [10] B. B. Jagannatha, J. B. H. Bouvier, and K. Ho, “Preliminary design of low-energy, low-thrust transfers to halo orbits using feedback control,” *Journal of Guidance, Control, and Dynamics*, Vol. 42, No. 2, 2019, pp. 260–271, 10.2514/1.G003759.
- [11] S. K. Singh, B. D. Anderson, E. Taheri, and J. L. Junkins, “Exploiting manifolds of L1 halo orbits for end-to-end Earth–Moon low-thrust trajectory design,” *Acta Astronautica*, Vol. 183, No. March, 2021, pp. 255–272, 10.1016/j.actaastro.2021.03.017.
- [12] Y. Sidhoum and K. Oguri, “Indirect Forward-Backward Shooting for Low-thrust Trajectory Optimization in Complex Dynamics,” *33rd AAS/AIAA Space Flight Mechanics Meeting, Austin, TX*, 2023.
- [13] H. Holt, N. Bernardini, N. Baresi, and R. Armellin, “Reinforced Lyapunov Controllers and Convex Optimisation for Low-thrust Lunar Transfers,” *33rd AAS/AIAA Space Flight Mechanics Meeting, Austin, TX*, 2023.
- [14] G. Mingotti, F. Topputo, and F. Bernelli-Zazzera, “Low-energy, low-thrust transfers to the Moon,” *Celestial Mechanics and Dynamical Astronomy*, Vol. 105, 2009, pp. 61–74.
- [15] R. Epenoy and D. Pérez-Palau, “Lyapunov-based low-energy low-thrust transfers to the Moon,” *Acta Astronautica*, Vol. 162, No. December 2018, 2019, pp. 87–97, 10.1016/j.actaastro.2019.05.058.
- [16] N. L. Parrish, E. Kayser, S. Udupa, J. S. Parker, B. W. Cheetham, and D. C. Davis, “Ballistic lunar transfers to near rectilinear halo orbit: Operational considerations,” *AIAA Scitech 2020 Forum*, 2020, p. 1466.
- [17] E. A. Belbruno and J. K. Miller, “Sun-perturbed Earth-to-Moon transfers with ballistic capture,” *Journal of Guidance, Control, and Dynamics*, Vol. 16, No. 4, 1993, pp. 770–775.
- [18] J. Kawaguchi, H. Yamakawa, T. Uesugi, and H. Matsuo, “On making use of lunar and solar gravity assists in LUNAR-A, PLANET-B missions,” *Acta Astronautica*, Vol. 35, No. 9–11, 1995, pp. 633–642.
- [19] S. T. Scheuerle, K. C. Howell, and D. D. C., “Low Thrust Augmentation for Ballistic Lunar Transfers,” *33rd AAS/AIAA Space Flight Mechanics Meeting, Austin, TX*, 2023.
- [20] J. A. Sims and S. N. Flanagan, “Preliminary Design of Low Thrust Interplanetary Missions,” *AAS/AIAA Astrodynamist Specialist Conference*, 1999.
- [21] P. E. Gill, W. Murray, and M. A. Saunders, “SNOPT: An SQP algorithm for large-scale constrained optimization,” *SIAM review*, Vol. 47, No. 1, 2005, pp. 99–131.
- [22] K. C. Howell and M. Kakoi, “Transfers between the Earth-Moon and Sun-Earth systems using manifolds and transit orbits,” *Acta Astronautica*, Vol. 59, No. 1–5, 2006, pp. 367–380, 10.1016/j.actaastro.2006.02.010.
- [23] A. Zanzottera, G. Mingotti, R. Castelli, and M. Dellnitz, “Intersecting invariant manifolds in spatial restricted three-body problems: Design and optimization of Earth-to-halo transfers in the Sun–Earth–Moon scenario,” Vol. 17, 2012, pp. 832–843, 10.1016/j.cnsns.2011.06.032.
- [24] R. Castelli, “Regions of prevalence in the coupled restricted three-body problems approximation,” *Communications in Nonlinear Science and Numerical Simulation*, Vol. 17, No. 2, 2012, pp. 804–816, 10.1016/j.cnsns.2011.06.034.
- [25] K. Yagasaki, “Sun-perturbed Earth-to-Moon transfers with low energy and moderate flight time,” *Celestial Mechanics and Dynamical Astronomy*, Vol. 90, No. 3, 2004, pp. 197–212.

- [26] Y. Qi, S. Xu, and R. Qi, “Gravitational lunar capture based on bicircular model in restricted four body problem,” *Celestial Mechanics and Dynamical Astronomy*, Vol. 120, No. 1, 2014, pp. 1–17, 10.1007/s10569-014-9554-7.
- [27] Y. Qi and S. Xu, “Optimal earth-moon transfers using lunar gravity assist in the restricted four-body problem,” *Acta Astronautica*, Vol. 134, No. January 2016, 2017, pp. 106–120, 10.1016/j.actaastro.2017.02.002.
- [28] K. Onozaki, H. Yoshimura, and S. D. Ross, “Tube dynamics and low energy Earth – Moon transfers in the 4-body system,” *Advances in Space Research*, Vol. 60, No. 10, 2017, pp. 2117–2132, 10.1016/j.asr.2017.07.046.
- [29] N. Bosanac, A. D. Cox, K. C. Howell, and D. C. Folta, “Trajectory design for a cislunar CubeSat leveraging dynamical systems techniques: The Lunar IceCube mission,” *AAS Astrodynamics Specialists Conference*, 2017, 10.1016/j.actaastro.2017.12.025.
- [30] W. Bing-wei and L. Yin-shan, “Low-energy Lunar Trajectories with Lunar Flybys,” *Chinese Astronomy and Astrophysics*, Vol. 42, No. 4, 2018, pp. 575–593, 10.1016/j.chinastron.2018.10.005.
- [31] K. Boudad, *Disposal dynamics from the vicinity of near rectilinear halo orbits in the Earth-Moon-Sun system*. PhD thesis, Purdue University Graduate School, 2019.

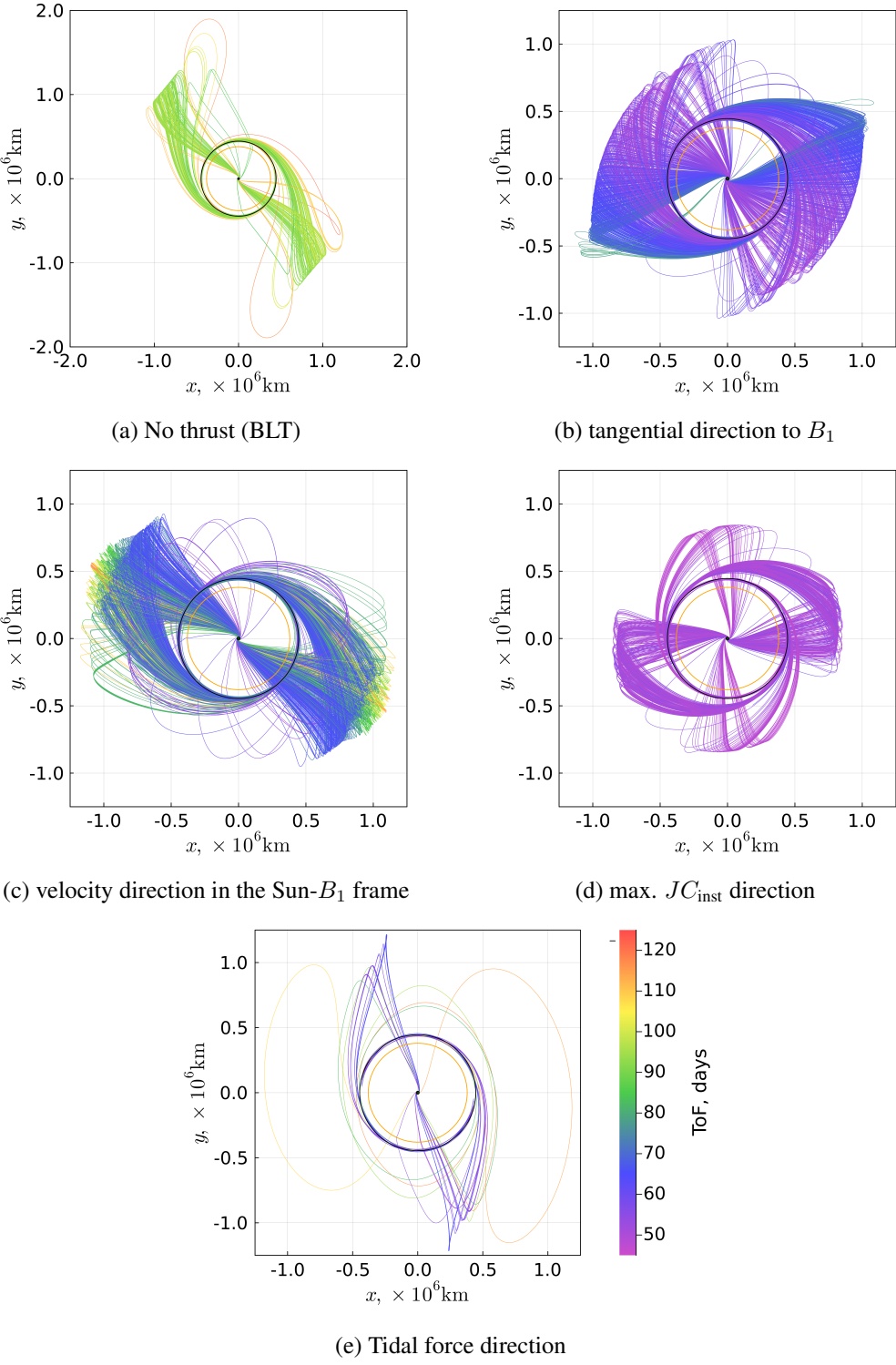


Figure 4: Feasible trajectories corrected from the initial guess candidates from each thrust policy. All trajectories are plotted in the Sun- B_1 frame. The yellow circle is the Moon orbit, the black dot at the center is B_1 , and the exterior black circle is the Earth-Moon L_2 . The origin is shifted to B_1 .

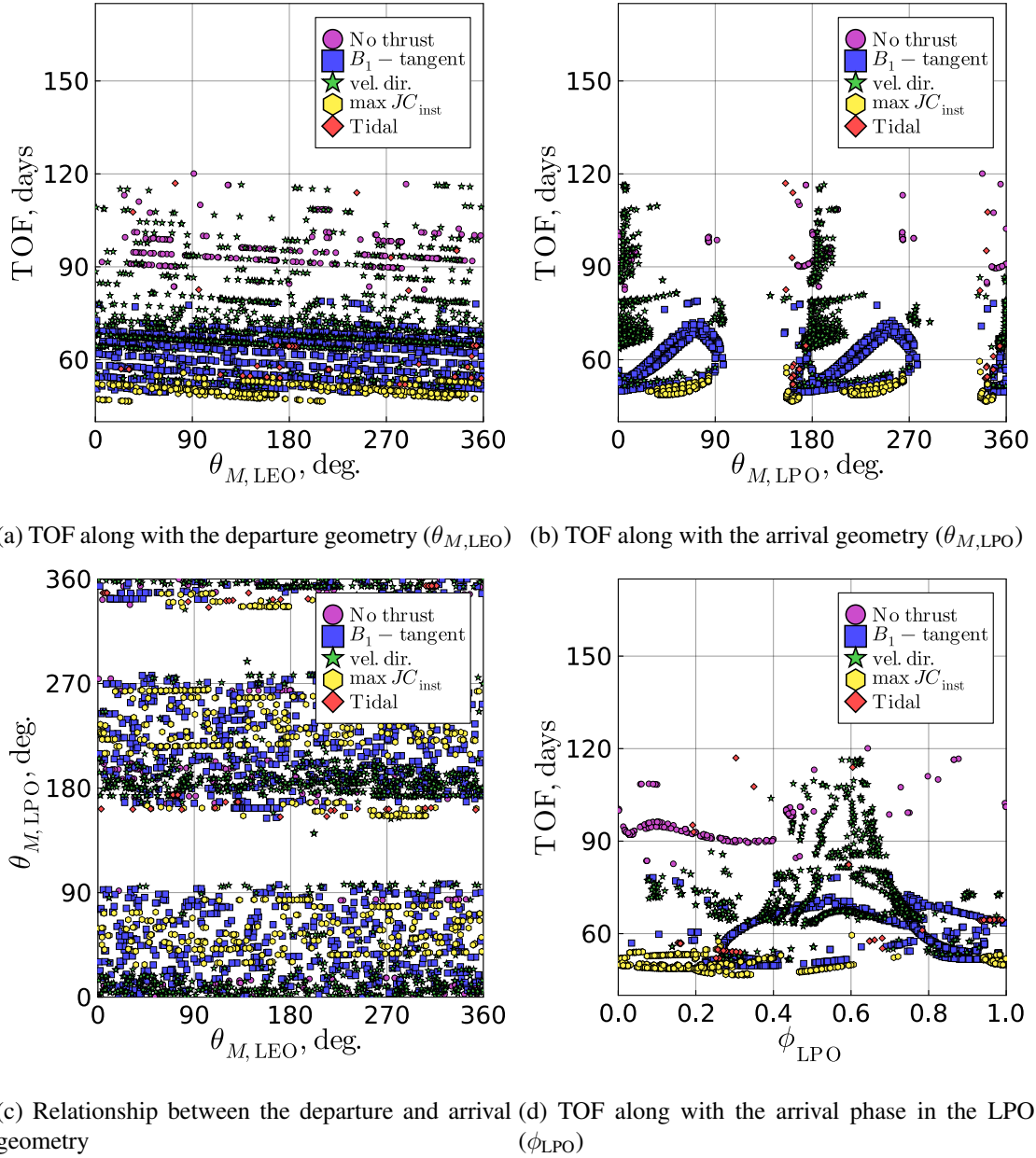


Figure 5: Departure and Arrival properties of the obtained trajectories

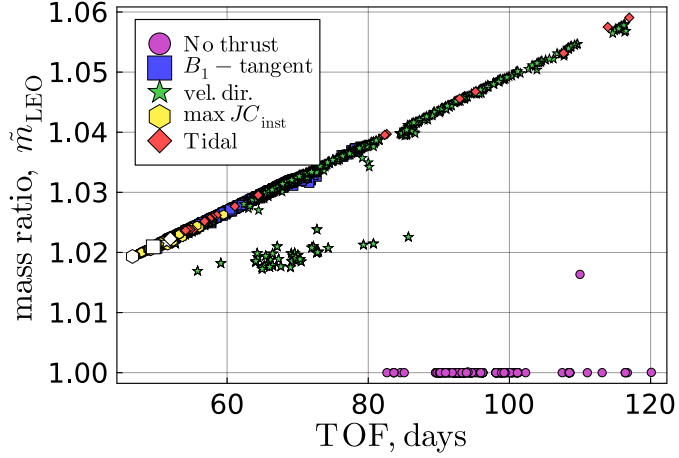


Figure 6: Relationship of the TOF and departure mass ratio for the corrected trajectories. Labels correspond to the pre-correction heuristic thrust policies for the corresponding initial guess. White markers indicate the minimum TOF solution for each thrust policy.

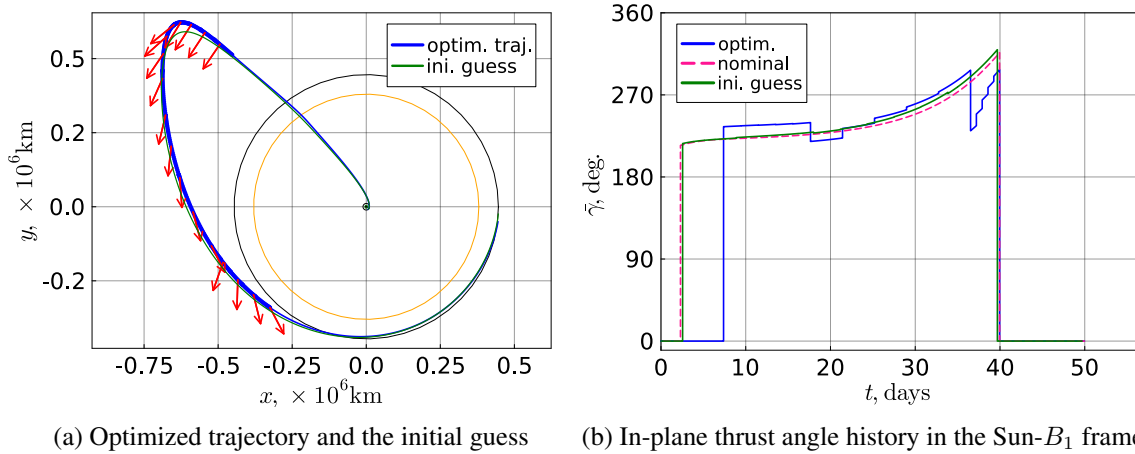


Figure 7: Optimized Earth-Moon transfer from the trajectory with thrust tangent to B_1 (TOF: 49.953 days, \tilde{m}_{LEO} : 1.0184)

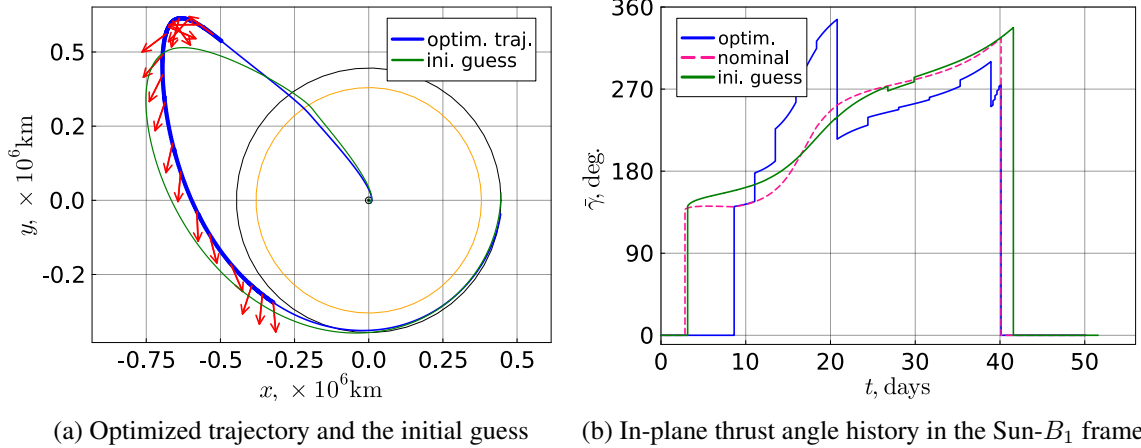


Figure 8: Optimized Earth-Moon transfer from the trajectory with thrust in velocity direction in the Sun- B_1 frame (TOF: 50.125 days, $\tilde{m}_{\text{LEO}} : 1.0178$)

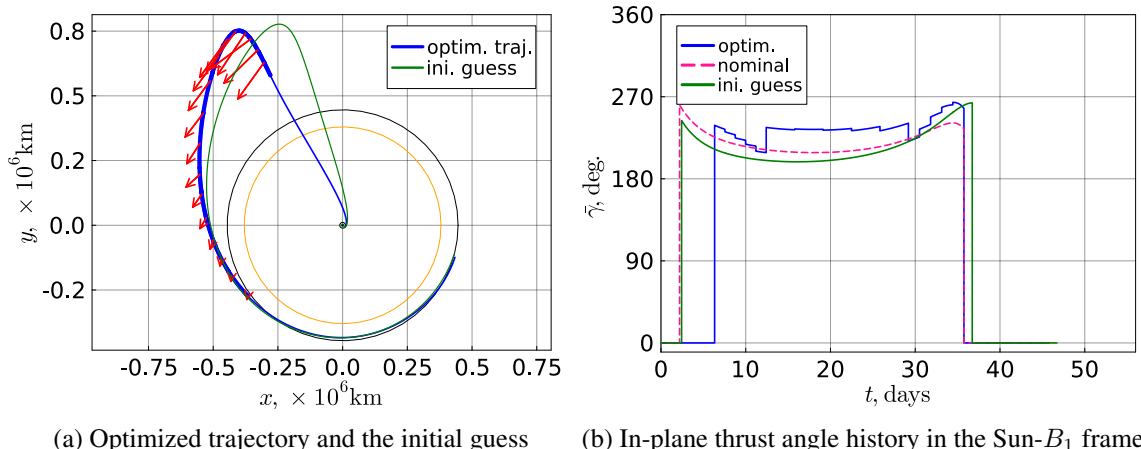
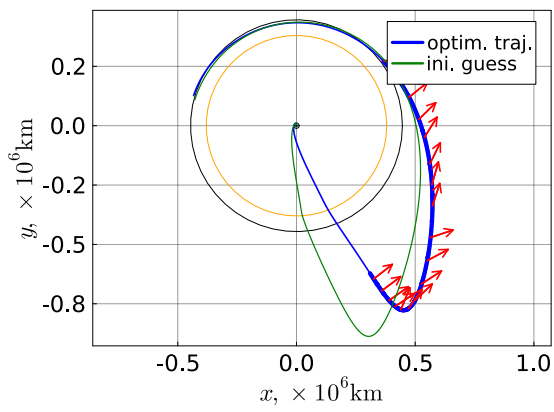
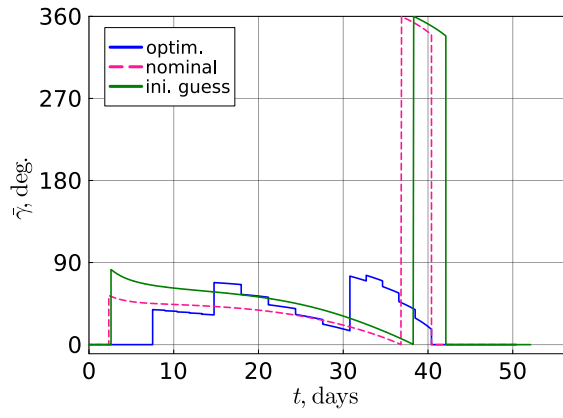


Figure 9: Optimized Earth-Moon transfer from the trajectory with thrust in max. JC_{inst} direction (TOF: 45.746 days, $\tilde{m}_{\text{LEO}} : 1.0166$)



(a) Optimized trajectory and the initial guess



(b) In-plane thrust angle history in the Sun- B_1 frame

Figure 10: Optimized Earth-Moon transfer from the trajectory with thrust in tidal force direction (TOF: 50.412 days, \tilde{m}_{LEO} : 1.0184)